ISSN 0016-7029, Geochemistry International, 2015, Vol. 53, No. 11, pp. 973–986. © Pleiades Publishing, Ltd., 2015.
Original Russian Text © V.L. Tauson, S.N. Rychagov, V.V. Akimov, S.V. Lipko, N.V. Smagunov, I.N. Gerasomov, R.G. Davletbaev, B.A. Loginov, 2015, published in Geokhimiya, 2015, No. 11, pp. 1000–1014.

Role of Surface Phenomena in Concentrating Incompatible Elements: Au in Pyrite from Hydrothermal Clays at Thermal Fields in Southern Kamchatka

V. L. Tauson[a], S. N. Rychagov[b], V. V. Akimov[a], S. V. Lipko[a], N. V. Smagunov[a], I. N. Gerasomov[a], R. G. Davletbaev[b], and B. A. Loginov[c]

[a] *Vinogradov Institute of Geochemistry, Siberian Branch, Russian Academy of Sciences, ul. Favorskogo 1a, Irkutsk, 664033 Russia*
e-mail: vltauson@igc.irk.ru

[b] *Institute of Volcanology and Seismology, Far East Division, Russian Academy of Sciences, bul'v. Piipa 9, Petropavlosk-Kamchatskii, 683006 Russia*
e-mail: rychsn@kscnet.ru

[c] *National Research University of Electronic Technology, proezd 4806 5, Zelenograd, Moscow, 124498 Russia*
e-mail: b-loginov@mail.ru

Received June 14, 2013; in final form, October 19, 2013

Abstract—The paper reports data on pyrite obtained using microscopic, physicochemical, and analytical techniques. The major mineral concentrating Au in clays at the Upper Koshelevskoe and East Pauzhetka hydrothermal fields is pyrite, which contains Au evenly distributed in its crystals (0.07–0.25 ppm) and Au bound to the surface of its crystals (0.8–6.8 ppm). The clear correlations between the concentration of equally distributed Au and the topological surface area of single crystals and the absence of correlations with the bulk specific BET surface area rule out purely adsorption mechanisms of Au accommodation at the surface of pyrite crystals, because otherwise the concentration of the minor element would have been proportional to the actual surface area but not the geometric one. In contrast to what is typical of high-temperature hydrothermal systems, at hydrothermal fields Au is an element highly compatible with pyrite. This may be explained by changes in the growth mechanisms of pyrite crystals and the transition to their growth via incorporation of colloid and subcolloid particles. Low-temperature pyrite in hydrothermal clays exhibits certain geochemical features important for exploration for gold deposits related to modern and ancient hydrothermal systems. This pyrite differs from higher temperature pyrite at ancient gold deposits in bearing sulfoxide sulfur species on the surface of its crystals instead of monosulfide species and also in having a less ordered and dense structure, higher porosity, and a globular topography of the surface of crystals.

Keywords: hydrothermal fields, Kamchatka, pyrite, gold, modes of Au occurrence, surface, typomorphism, typochemism

DOI: 10.1134/S0016702915110051

INTRODUCTION

Hydrothermal clays occurring at the surface of hydrothermal fields are, in a sense, natural laboratories, at which "experiments" proceed at certain temperatures and pressures in very complicated systems (Rychagov et al., 2010). These clays are of remarkable interest as a source of information on the fluid regime of ore-forming hydrothermal–magmatic systems in island arcs and on the behavior of various elements in these systems. The behavior of some elements often looks like very unusual. For example, Ti, which is traditionally thought to be an element of the lowest geochemical mobility, can become mobile under certain conditions. Being incompatible with pyrite, Ti (and some other elements) is accommodated in nanometer-thick films on the surface of pyrite crystals, with the Ti concentrations in these films reaching 5 at % (Rychagov et al., 2012). Generally speaking, Au is also an element incompatible with pyrite (Tauson et al., 2011), but we continue to stress that this incompatibility is relative when speaking about defects in the crystal structures of mineral phases (Tauson, 2005). An element may be compatible and be readily accommodated in a defective crystal or, in the absence of controlling defects, be incompatible with the same crystalline matrix but devoid of defects, and thus the element enrich the surface of the phase. The speciation of trace elements should be taken into account in mineralogical and geochemical studies because of the dualistic character of the distribution coefficients of these elements, which can differ by as much as a few orders of magnitude for the structural and surface-related modes of occurrence of the element (Tauson et al., 2011).

Table 1. Characteristics of pyrite panning samples from hydrothermal clays at thermal fields in southern Kamchatka that contained enough single pyrite crystals for their SSADSC analysis

Sample number	Sampling site	Sampling depth, cm	Characteristics of pyrite crystals		
			size of crystal edges, mm	shape	surface
VK-1/09-2	Upper Koshelevskoe thermal field, central part, prospecting pit	30–50	≤0.5	{100}, {100} + {111}	Clean, no striated crystal faces or very coarse striation
VK-1/09-3	Same	50–70	≤0.6	{100}, {100} + {111}, @реже {hkk}	Clean, striation on some face
VPP-1/08-2 shkh	East Pauzhetka thermal field, dug hole	25–50	From ≤0.6 (mostly) to 1.55	{100 }(mostly), @реже{100} + {111}	Often brown (oxidized), coarse striation
VPP-1/08-3 shkh	Same	50–70	From ≤0.6 (mostly) to 1	Same	Clean, coarse and uneven striation
VPP-1/08-4 shkh	″	70–90	From ≤0.5 (mostly) to 1.5, aggregates of small blocks in a single crystal	″	Same
VPP-1/08-5 shkh	″	90–110	From ≤0.5 (mostly) to 1.5	″	″

When studying clays at thermal fields in southern Kamchatka, we obtained data on Au concentrations in the clays and monomineralic pyrite fractions from various sections of the Lower Koshelevskoe and Pauzhetka geothermal fields and sites of thermal activity in the Kambal'nyi volcanic range (Rychagov et al., 2008). The Au concentrations of pyrite were determined to be either much higher than in the clays or comparable with them. The Au concentrations of the pyrite vary within more than two orders of magnitude: from 0.001 to 0.2 ppm. The reason for such a great dispersion of the Au concentrations of the pyrite is so far uncertain, but it is clear that these variations can hardly be explained by the variations in the composition of the thermal waters. The dispersion of the concentrations is comparable with the dispersion of the average values of selected size fractions pyrite crystals and may thus be of the same nature. For example, the average concentrations of equally distributed Au in thoroughly studied large selections of pyrite from wall-rock metasomatites at the Zun-Kholba deposits in the Eastern Sayan Range increases from 0.15 to 116 ppm at the average sizes of the crystals (edges of cubes) decreasing from 1.7 to 0.4 mm (Tauson and Lipko, 2013). It was suggested that pyrite crystallizing in the supergenesis zone at hydrothermal deposits plays a significant role in the accumulation and redistribution of base metals, Au, Hg, and some other elements (Rychagov et al., 2008). The bulk concentrations do not shed light onto the role of pyrite in Au concentrating and, hence, also on the efficiency of the subaquatic sulfide barrier of gold–base metal specifics. The likely reason is that the bulk concentrations do not provide any insight into the mechanism of gold incorporation into the mineral phase. In view of this, herein we focus attention on the role of surface phenomena in Au concentrating and the interplay of various mechanisms of Au accommodation in pyrite crystals as a structurally bound species and those related to crystal surface, as nanometer-sized film phases.

MATERIALS AND METHODS

Hydrothermal clay samples were collected in dug holes 2.4 m deep, with sampling sites spaced 20 cm apart in the vertical section of each hole. The clays were analyzed by XRF on a S4 PIONEER at the Analytical Center of the Institute of Volcanology and Seismology, Far East Division, Russian Academy of Sciences. The mineralogy and geochemistry of the clays were described in much detail in (Rychagov, 2008, 2012). Clay samples from each layer of the vertical section were washed to obtain gray concentrate of heavy minerals. The heavy fraction of the concentrate contained more than 90% pyrite and minor amounts of quartz and magnetite. Not all of the samples contained enough pyrite crystals of various size and high quality (sufficient for applying the method of statistical selections of analytical data on single crystals, SSADSC; Tauson and, 2011; Tauson and Lipko, 2013). The most common reason for the unsuitability of the samples was the small sizes of the individual crystals (≤~0.1 mm) and crystal aggregates and the poorly pronounced faceting of the individual crystals. The sizes and dominant faceting of the crystals are listed in Table 1.

When studying the crystals, we applied techniques of scanning microprobe microscopy, low-temperature

nitrogen adsorption BET, and X-ray photoelectron spectroscopy XPS. Our studies by atomic force microscopy AFM were carried out using a SMM-2000 (Russia) scanning multimicroscope at the Institute of Volcanology and Seismology, Far East Division, Russian Academy of Sciences, and by tunnel microscopy, STM, using analogous equipment at the same institution. The AFM images were obtained in contact mode; the curvature radius of the scanning needle was 30 nm, and the maximum controllable resolution was approximately 2.5 nm in the *XY* plane and 1 nm along *Z*. The STM images were obtained with a needle made of Pt (analytical-grade) drawn wire, whose bend radius was 1 nm. The spacing between the needle and sample in the course of scanning was 1–2 nm. The specific surface and porosity were determined on a SORBOTOMETER-M (Russia) at the Vinogradov Institute of Geochemistry, Siberian Branch, Russian Academy of Sciences, in a number of samples more or less suitable for these measurements it terms of mass and purity. The X-ray photoelectron spectra (XPS) were recorded on a LAS-3000 (Riber, France) at the Central Institute of Geological Exploration for Base and Precious Metals (TsNIGRI). The spectra were excited by AlK_α nonmonochromatic X-ray radiation (1486.6 eV). The internal standard (to account for the electrostatic charge) was line 1s of carbon C, whose bond energy in hydrocarbons (contaminants) is 285.0 eV. Selected spectral lines were scanned in 0.1 eV increments. We have recorded spectra of both original crystals and crystals after their ion milling with a beam of Ar^+ ions for 0.5 h at a rate of ~6 nm/min. The peaks were processed with the CasaXPS software. The fine structure of pyrite crystals was studied by X-ray powder diffraction XRD on a D8 ADVANCE (BRUCKER) diffractometer at the Vinogradov Institute. We determined the unit cell parameters and fine structure of crystals: the size of the crystallites (blocks) and the level of lattice microdeformations.

The modes of Au occurrence were determined by the SSADSC method (Tauson et al., 2011; Tauson and Lipko, 2013). Single pyrite crystals of various size were analyzed for Au by atomic absorption spectrometry with a graphite atomizer after their dissolution in HCl + $KClO_3$ at heating. The analysis was carried out using a Perkin-Elmer Model 503 atomic absorption spectrometer equipped with a deuterium background corrector and an HGA-74 graphite furnace operating in argon flow mode. The detection limit for Au was 0.3 μg/l (0.03 ppb), and the analytical errors were ±12%. Selections of crystals were formed in compliance with the following rules: (1) the crystals should be holohedral, with clean faces, showing minimum contamination with silicate and other nonsulfide materials; (2) the number of the individual crystals should be at a maximum (thereby all crystals should meet quality requirements), and the crystals should lie within an as narrow as possible size (mass) range; (3) each of the analyzed samples in which the structural component of its Au admixture was analyzed should comprise no less than four size fractions of pyrite crystals; and (5) the mass of any crystal should be no lower than 0.1 mg. All concentration values lower than three Au detection limits were rejected. Not all of our samples met these requirements. The most reliable results were obtained on two samples from the Upper Koshelevskoe thermal field and four samples from the East Pauzhetka thermal field. Since we were interested only in two modes of Au occurrence in the mineral (structural and surface-related), it was interesting to examine the distribution of Au concentrations in these two modes. The original selection consisted of 44–79 crystals of various size. In processing the analytical data on the crystals, the whole data set was subdivided into intervals according to crystal masses in such a way that all of the intervals comprised similar numbers of crystals. We did our best to adhere to the rule of an as small as possible scatter in the crystal masses, with regard for the quality of the inner statistics of the selections and the representativeness of the size fractions. Then we determined the average concentration for each interval and the mean square deviation *s*. Values greater than 1*s* were then rejected as not meeting the criterion of an even distribution. Negative deviation (<–1s) were left in the selection because these crystals could in principle contain any low concentrations of the structural admixture. After this we determined the new mean values and the standard deviation of the mean ±σ. During the final phase of our study, we applied a certain procedure to distinguish the structural mode from those somehow related to the surface. For this purpose we introduced a criterion according to which each concentration value C_{Au} within a given range of the size (mass) of the crystals should be rejected if this value was higher than $\overline{C}_{Au} + 30\%\overline{C}_{Au}$, which specified the possible variations in the concentration of the structure mode (Tauson and Lustenberg, 2008). Then we determined the average concentrations of evenly distributed Au in each size fraction ($\overline{C}_{Au} \pm \Delta$) corresponding to the average mass of the crystal $\overline{m}$ and the specific surface of the average crystal in a given size fraction: $\overline{S}_{уд} = l\overline{r}^2/\overline{m}$. The shape of the crystal was approximated by a cube with edges $\overline{r}$ (*l* is the shape factor).

If the number of the size fractions was high enough (≥4), the Au structural admixture could be determined from dependences of the form $\overline{C}_{Au} = ke^{n\overline{S}_{sp}}$ derived for the selections. Extrapolation of $\overline{C}_{Au}$ to $\overline{S}_{sp}$ leads to a value $\overline{C}_{Au} = k$, which characterizes a virtual crystal of infinite mass. It corresponds to the concentration of structural Au in pyrite accurate to ±30% (Tauson and Lustenberg, 2008). Adsorbed Au (and Au in any mode related to the surface of the crystals) is also evenly distributed between the crystals (but not through their volumes). It was evaluated by the formula $\overline{C}_{sur} =$

Table 2. Analytical data on selected size fractions of pyrite crystals [{100} from hydrothermal clays at the Upper Koshelevskoe (samples labeled VK) and East Pauzhetka (VPP) geothermal fields in southern Kamchatka

Sample number	Number of crystals (initial–final select.)	Characteristics of final selection						Au concentration, ppm**		
		number of crystals	weight range, mg	$\bar{m}$, mg	$\bar{r}$, mm	$\bar{S}_{◆◆}$, mm^2/g	$\bar{◆}_{Au} \pm \Delta$, ppm	$\bar{C}_{tot.}$	C_{str}	$\bar{C}_{sur}$
VK-1/09-2	50–36	8	0.11–0.23	0.18	0.330	3.630	6.0 ± 1.6	6.2	0.13	2.6
		9	0.24–0.27	0.26	0.373	3.211	3.2 ± 1.2			
		9	0.28–0.44	0.38	0.424	2.839	3.0 ± 0.9			
		10	0.45–0.7	0.56	0.482	2.489	1.6 ± 0.4			
VK-1/09-3	52–33	9	0.07–0.14	0.12	0.288	4.148	18.1 ± 4.2	13.4	0.25	6.8
		8	0.15–0.22	0.19	0.336	3.565	11.2 ± 3.2			
		8	0.23–0.31	0.29	0.387	3.099	4.9 ± 1.2			
		8	0.34–0.75	0.51	0.467	2.566	3.9 ± 1.3			
VPP-1/08-2 shkh	52–35	9	0.16–0.3	0.28	0.383	3.143	4.4 ± 0.9	1.6	0.12	0.9
		8	0.31–0.62	0.52	0.470	2.549	2.4 ± 0.6			
		8	0.64–1.87	1.59	0.683	1.760	0.98 ± 0.15			
		10	1.9–4.57	3.07	0.850	1.412	0.57 ± 0.06			
VPP-1/08-3 shkh	44–34	8	0.14–0.26	0.20	0.342	3.509	7.2 ± 2.1	1.8	0.11	0.8
		9	0.3–0.52	0.38	0.424	2.839	3.0 ± 0.8			
		8	1.13–2.45	1.69	0.697	1.725	0.93 ± 0.15			
		9	2.9–7.26	4.59	0.972	1.235	0.46 ± 0.05			
VPP-1/08-4 shkh	59–42	10	0.1–0.14	0.12	0.288	4.148	10.1 ± 4.9	5.4	0.07	2.0
		10	0.15–0.2	0.17	0.324	3.705	7.3 ± 1.4			
		8	0.23–0.34	0.26	0.373	3.211	4.8 ± 1.2			
		6	0.37–0.86	0.56	0.482	2.489	1.7 ± 0.4			
		8	1.02–2.85	1.73	0.702	1.709	0.49 ± 0.05			
VPP-1/08-5 shkh	79–57	8	0.11–0.2	0.17	0.324	3.705	6.4 ± .9	3.0	0.17	1.3
		11	0.22–0.29	0.25	0.368	3.250	4.0 ± 0.6			
		13	0.32–0.48	0.40	0.431	2.787	2.8 ± 0.5			
		8	0.55–0.89	0.72	0.524	2.288	1.6 ± 0.4			
		9	0.95–1.39	1.19	0.620	1.938	0.87 ± 0.14			
		8	1.46–5.96	2.61	0.805	1.490	0.86 ± 0.33			

* $\bar{C}_{tot.}$ is the total concentration $\frac{\Sigma◆_i m_i}{\Sigma m_i}$; C_{str} is the concentration of the structural mode (at $\bar{◆}_{Au}$ extrapolation to zero $\bar{S}_{spec}$), and $\bar{C}_{sur}$ is the average concentration of surface-related modes of Au occurrence.

$\frac{\Sigma\left(\bar{C}^b - C_{str}\right) n^b \bar{m}^b}{\Sigma n^b \bar{m}^b}$, in which $\bar{C}^b = \bar{C}_{Au}$ is the average concentration of evenly distributed Au in each size fraction b of n pyrite crystals having an average mass $\bar{m}$ (Tauson and Lustenberg, 2008; Tauson et al., 2011).

RESULTS AND DISCUSSION

We applied the SSADSC technique to determine the concentrations of structural C_{str} and surface-related $\bar{C}_{sur}$ Au in pyrite (Table 2). They reflect highly deterministic dependences of the average concentration of evenly distributed Au in a size fraction on the specific surface area of an average crystal in this fraction (R^2 = 0.934–0.997). Such clear dependences cannot be a consequence of simple Au adsorption on the surface of pyrite crystals. This is obvious from the comparison of data on two samples that have appreciably different BET specific surface areas and, at the same time, show

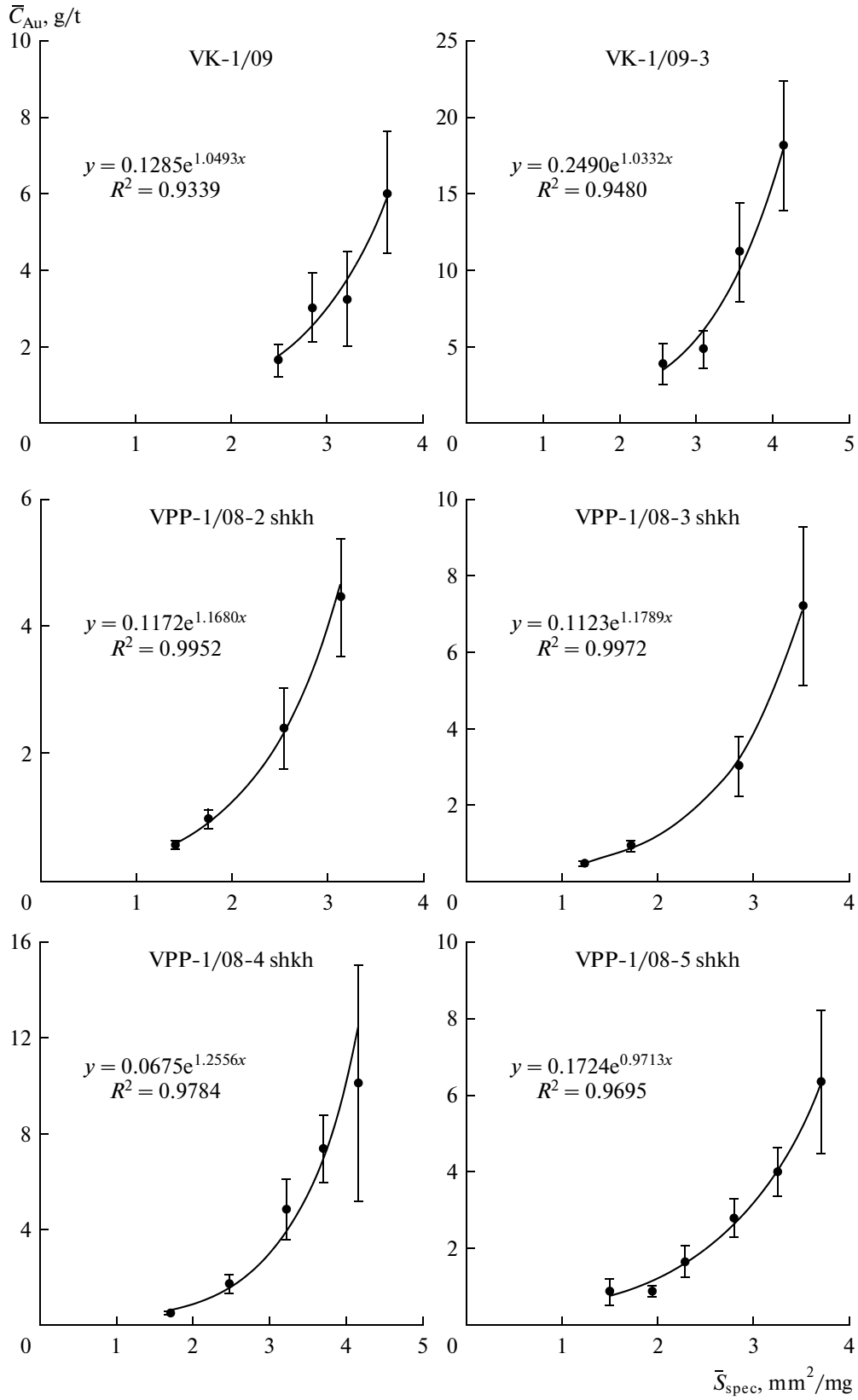

Fig. 1. Dependence of the average concentration of evenly distributed Au on the specific surface of an average crystal in size fractions of pyrite from the Upper Koshelevskoe (VK) and East Pauzhetka (VPP) thermal fields.

Table 3. Physicochemical characteristics of pyrite samples

Sample	Size fraction, mm	Amount of material, g	BET specific surface, mm^2/mg		Specific volume of pores, mm^3/mg	Average size of pores, nm
			single-spot	multispot		
VK-1/09-03	0.63–0.2	6.6092	580	576	0.001	22
VPP-1/08-2shkh*	0.63–0.2	3.9847	6410	–	0.003	n.d.

* Contaminates with small particles of nonore minerals.

Table 4. Characteristics of the surface of pyrite crystals and features on it deduced from AFM data

Sample	Size parameters of surface and its features, nm*				
	root-mean-squared roughness	@глобули и частицы		pores	
		lateral size *XY*	height *Z*	diameter	depth
VK-1/09-2	$\frac{8-17}{11}$	$\frac{100-900}{400}$	$\frac{10-90}{30}$	$\frac{90-600}{280}$	$\frac{12-45}{25}$
VPP-1/08-2 shkh	$\frac{4-10}{6}$	$\frac{80-270}{160}$	$\frac{10-30}{20}$	$\frac{40-130}{75}$	$\frac{10-35}{20}$

* Range and average.

Table 5. X-ray diffraction characteristics of pyrite crystals

Sample	a_0, nm	D, nm	$\sqrt{\langle \varepsilon^2 \rangle} \times 10^3$
VK-1/09-2	0.54156	220	0.2
VK-1/09-3	0.54159	230	0.2
VPP-1/08-2 shkh	0.54158	170	0.1
VPP-1/08-3 shkh	0.54158	190	0.1
VPP-1/08-4 shkh	0.54158	200	0.2
VPP-1/08-5 shkh	0.54157	210	0.2

a_0 is the unit cell parameter under normal conditions determined accurate to ±0.00001 nm; D is the size of the blocks (coherent scattering domains) determined accurate to ±10 nm; and $\sqrt{\langle \varepsilon^2 \rangle} \times 10^3$ is the relative RMS value of structural microdeformations.

similar $\overline{C}_{Au}$ dependences on $\overline{S}_{sp}$ and also follows from a pattern of Au behavior opposite to what could be expected based on surface characteristics (Tables 2, 3). Microscopical characteristics of the surfaces of the two samples are presented in Table 4 and were estimated based on AFM images at various magnification. The surface has a globular and porous "topography" (Figs. 2–4), shows flattened globules and particles and alternating densely packed and loose surface structures. The AFM images provide additional information on the structure of the surface of the pyrite crystals. The most typical "landforms" are colloform botryoidal, globular, pseudoglobular, and layered micrometer- and nanometer-sized structures (Fig. 5). Locally the structures show ultramicroscopic layering, with layers a few nanometers thick. The structural characteristics of the samples are only insignificantly different (Table 5). The unit-cell parameter is 0.54158 ± 0.00001 nm, the discrete blocks (domains of coherent scattering) vary from 170 to 230 nm, which is generally consistent with AFM data (Table 4). The minute disturbances of the structure are insignificant, as can in principle be expected from low-temperature crystals that do not contain elevated concentrations of any admixtures. Table 6 reports XPS data

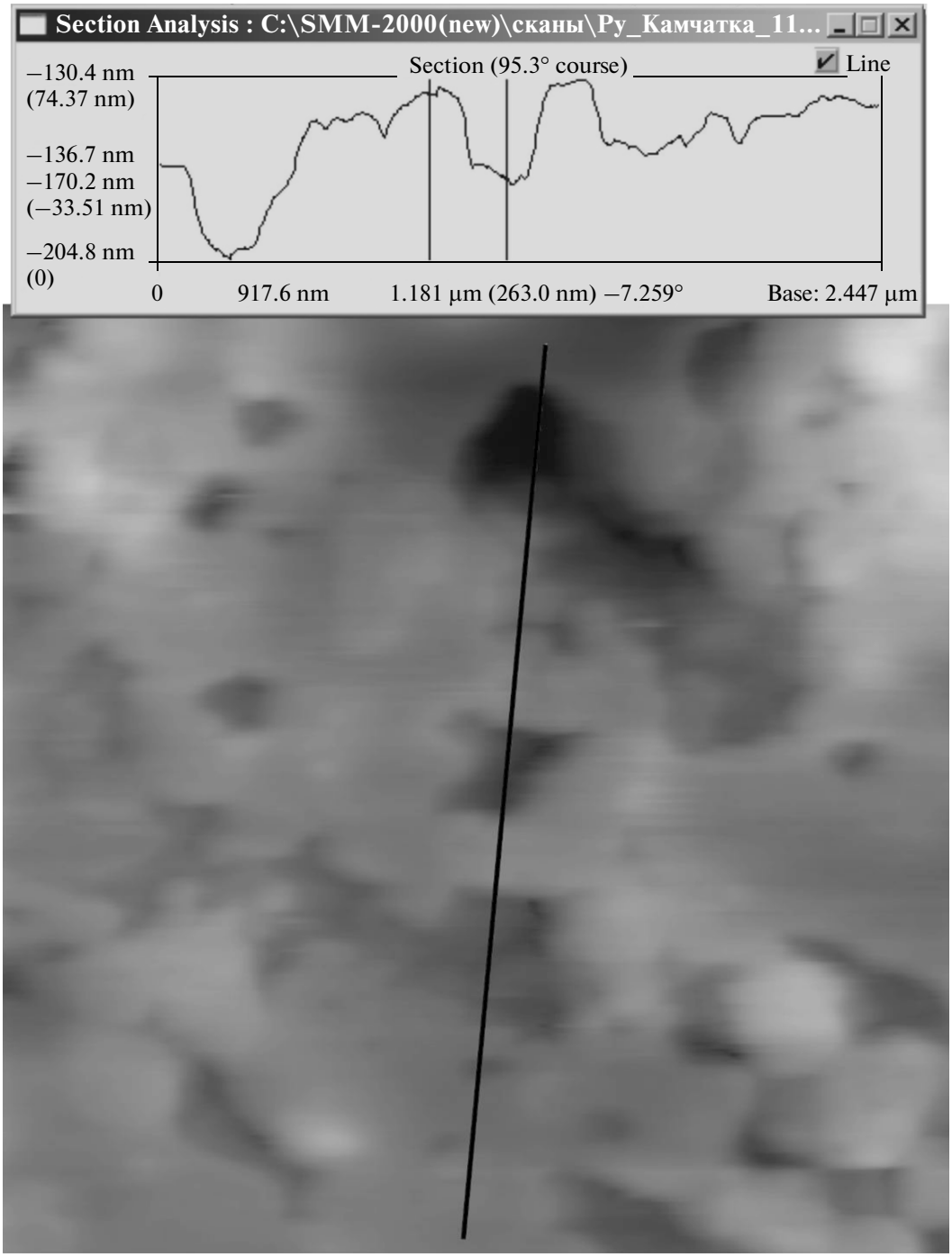

Fig. 2. AFM image of the surface of a face of a pyrite crystal, sample VK-1/09-2. Image size: 2.578 × 2.578 × 0.122 μm. The profile runs through two large pores 30 nm deep.

on pyrite from the East Pauzhetka thermal field. The spectra of all analyzed samples are of poor quality because of surface contaminations and because it is difficult to hand-pick a sufficient number of crystals of appropriately good faceting and similar size. When interpreting the results, we utilized data from (Tauson et al., 2008, 2012). A certain ambiguity thereby stems from the not always good enough quality of the spectra and from the fact that it is difficult to carry out ion milling under very closely similar conditions. Nevertheless, it is evident that the surface of pyrite crystals is covered mostly by sulfoxides, with bi- and trivalent iron and with sulfate and sulfide sulfur. "Pyrite" iron, which is bound to the disulfide ion, sometimes appears only after ion milling (Fig. 6), i.e., the surface is fairly densely covered by a film of sulfoxide phases ≤100–200 nm thick.

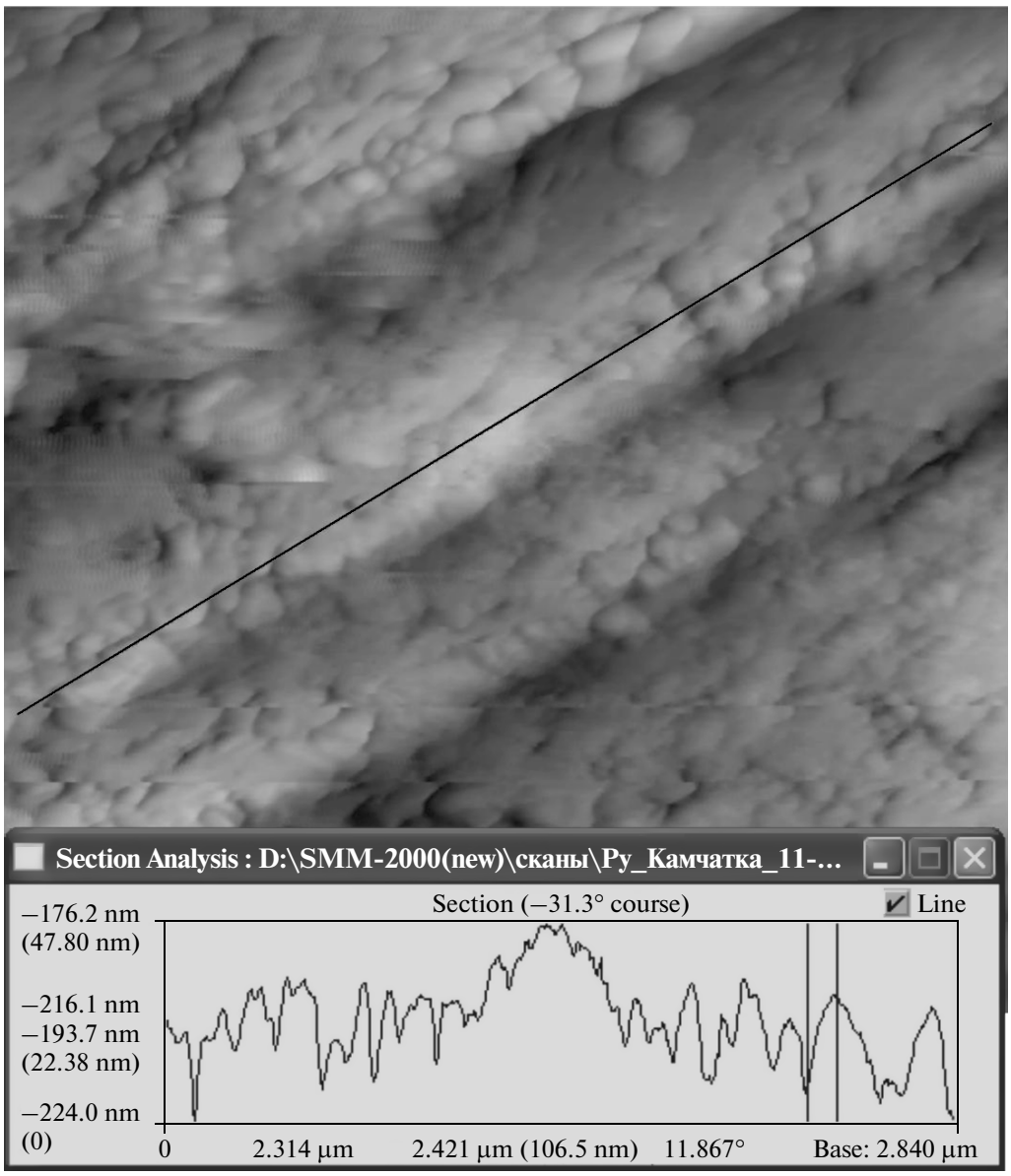

Fig. 3. AFM image of the surface of a face of a pyrite crystal, sample VPP-1/08-2 shkh. Image size: 2.5 ×2.5 × 0.098 μm. The image shows the globular structure of the surface with globules of various size, 200 nm on average.

Some uncertainties concerning sample VPP-1/08-4, whose Fe(II)-S_2 peak notably diminished after ion milling, may likely be explained by the transformation of sulfite and/or thiosulfite in the course of ion milling, as follows from the remarkable increase in the Fe(III) sulfate concentration. Perhaps Fe(III) in some samples was formed as a consequence of ion milling of the surface by Ar^+ ions because of Fe^{2+} oxidation by S^- ion radicals (Tauson et al., 2008). The samples are characterized by the absence of monosulfides sulfur, whose bond energy is ~161 eV and whose peak is clearly seen in all high-temperature pyrite samples (Tauson et al., 2008; Tauson and Lipko, 2013).

Table 7 reports the calculated Au concentrations in hydrothermal clays; the only explanation of these concentrations is that Au is contained in pyrite. The calculations were carried out using data from Table 7 and analytical data on the bulk sulfur concentrations of the samples. We assumed that all sulfur is contained in pyrite. Since the system can also contain other sulfur-bearing species, the estimates in Table 7 should be regarded as the maximum possible values. We did not distinguish between surface-related sulfur species belonging to pyrite itself (S_2^{2-}) and to surface phases (SO_3^{2-}, SO_4^{2-}) and believed that they belong to nonauto-

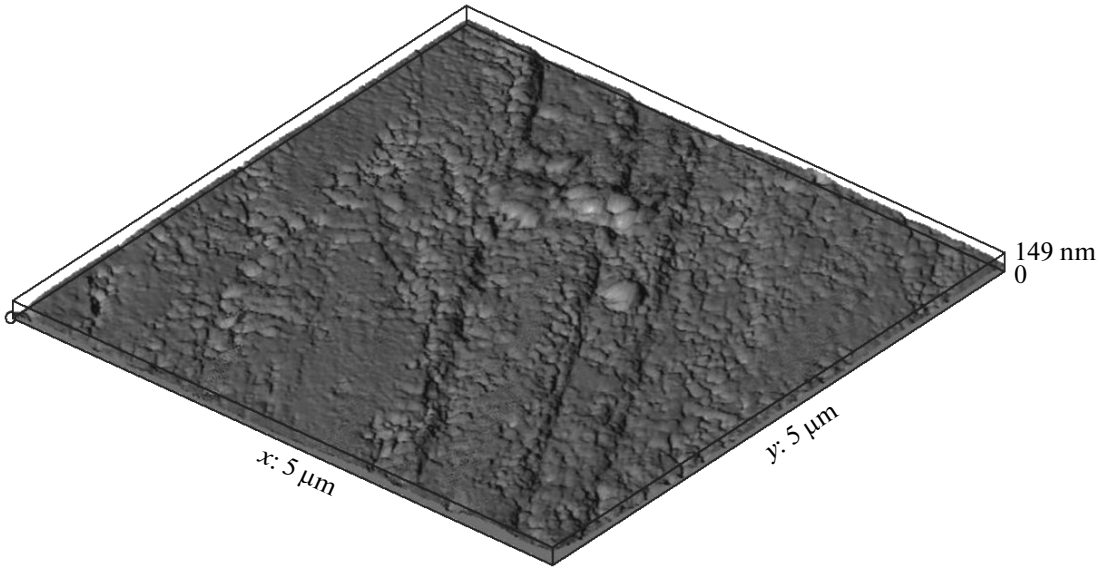

Fig. 4. 3D AFM image of the surface of a face of a pyrite crystal, sample VPP-1/08-2 shkh. Image size: 5 × 5 × 0.149 μm.

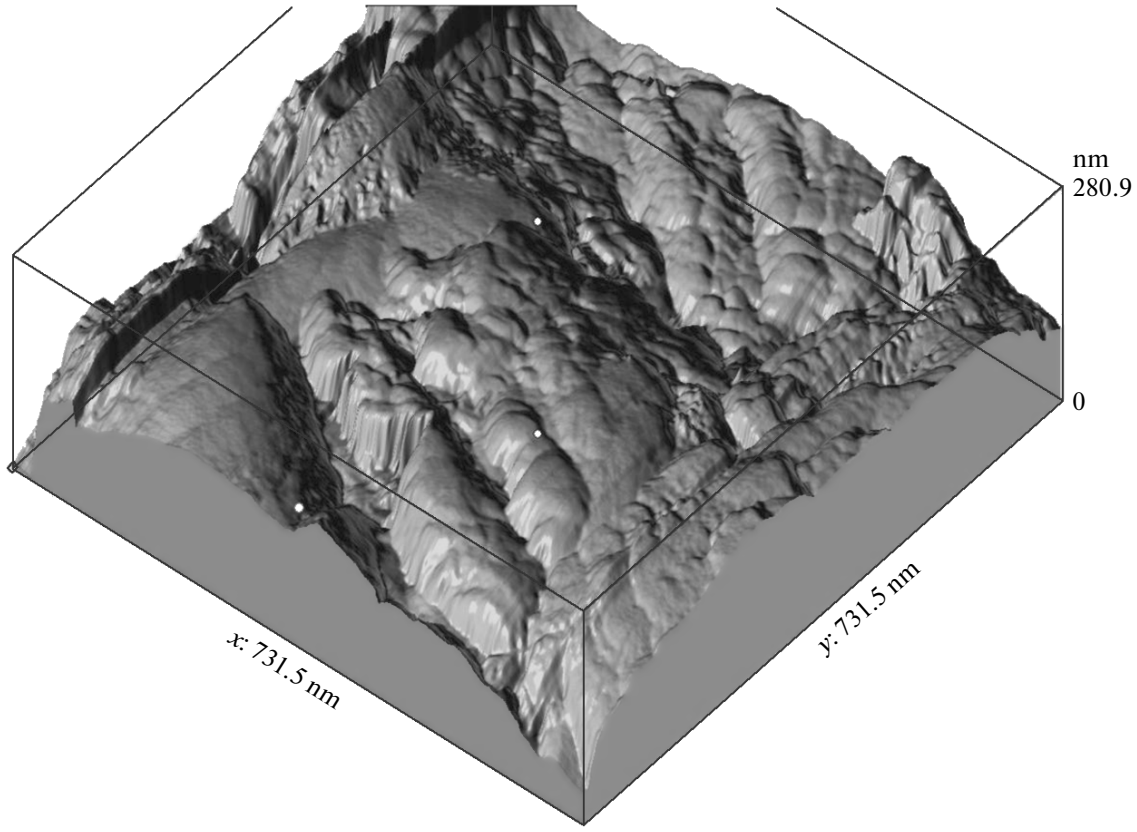

Fig. 5. STM image of the surface of a pyrite crystal from hydrothermal clay of the Upper Koshelevskoe thermal field. The size of the scanned surface is 731.5 × 731.5 × 280.9 nm.

nomous phases that are inseparable from pyrite by definition (Tauson et al., 2008; Tauson and Lipko, 2013).

As can be seen in Table 7, the bulk Au concentrations determined in the clays can be explained by the presence of Au-bearing pyrite alone. It is important to stress that the structural (volumetric) mode alone is able to account for from ~5 to 60% of the bulk Au concentration. As expected (see the Introduction), an important role is played by the size distribution of the pyrite crystals. The finest fractions are richer in Au

Table 6. XPS data on pyrite from the East Pauzhetka thermal field

Sample	Photoelectron pea	E_b, eV	Half-width, eV	Identification of the peak**	Mole fraction***
VPP-1/08-02 shkh	Fe $2p_{3/2}$	711.5	3.0	Fe(II)–S, –O; Fe(II)–SO_3	0.72
		714.0	3.5	Fe(III)–SO_4	0.28
	S $2p_{3/2}$	163.4	2.7	S_2^{2-}	0.34
		166.1	4.0	SO_3^{2-}	0.19
		169.2	4.0	SO_4^{2-}	0.47
Same*	Fe $2p_{3/2}$	707.3	2.9	Fe(II)–S_2	0.33
		710.0	4.0	Fe(II)–S, –O	0.42
		713.1	3.5	Fe(III)–SO_4	0.25
	S $2p_{3/2}$	162.7	3.0	S_2^{2-}	0.63
		168.5	3.2	SO_4^{2-}	0.37
VPP-1/08-3 shkh	Fe $2p_{3/2}$	707.1	4.0	Fe(II)–S_2	0.2
		711.5	3.8	Fe(II)–S; Fe(II)–SO_3, –SO_4	0.8
	S $2p_{3/2}$	162.1	2.2	S^{2-}, S_2^{2-}	0.28
		164.1	2.6	S_n^{2-}, SO_3^{2-}	0.4
		168.7	2.7	SO_4^{2-}	0.32
Same*	Fe $2p_{3/2}$	708.6	2.8	Fe(II)–S_2	0.15
		711.5	4.0	Fe(II)–S, –O; Fe(II)–SO_4	0.61
		714.5	3.6	Fe(III)–SO_4	0.24
	S $2p_{3/2}$	163.7	3.7	S_2^{2-}	0.56
		168.7	2.5	SO_4^{2-}–Fe(II)	0.25
		170.7	2.4	SO_4^{2-}–Fe(III)	0.19
VPP-1/08-4 shkh	Fe $2p_{3/2}$	708.2	3.7	Fe(II)–S_2	0.16
		711.2	4.0	Fe(II)–S; Fe(II)–SO_3	0.73
		713.9	2.4	Fe(III)–SO_4	0.11
	S $2p_{3/2}$	162.1	3.4	S^{2-}, S_2^{2-}	0.33
		167.5	3.1	$S_2O_3^{2-}$, SO_3^{2-}	0.52
		169.0	2.0	SO_4^{2-}	0.15
Same*	Fe $2p_{3/2}$	707.4	3.1	Fe(II)–S_2	0.05
		709.5	4.7	Fe(II)–S, –O; Fe(II)–SO_4	0.25
		712.7	3.0	Fe(III)–SO_4	0.7
	S $2p_{3/2}$	163.5	2.0	S_2^{2-}	0.3
		168.6	3.0	SO_4^{2-}–Fe(II)	0.49
		170.2	2.0	SO_4^{2-}–Fe(III)	0.21
VPP-1/08-5 shkh	Fe $2p_{3/2}$	709.8	2.3	Fe(II)–S, –O; Fe(II)–SO_4	1
	S $2p_{3/2}$	163.3	3.0	S_2^{2-}	0.57
		168.9	3.3	SO_4^{2-}	0.43
Same*	Fe $2p_{3/2}$	708.1	3.0	Fe(II)–S_2	0.44
		710.4	3.0	Fe(II)–S, –O	0.34
		712.9	2.9	Fe(III)–SO_4	0.22
	S $2p_{3/2}$	163.5	3.3	S_2^{2-}	0.71
		169.0	3.8	SO_4^{2-}	0.29

* Ion milling with Ar^+ for 0.5 h.

** With regard for atomic concentrations of Fe and S species, S_n^{2-}- ($n > 2$) is the polysulfide ion, S_2^{2-} – is the disulfide ion, and S^{2-} is the sulfide ion; Fe(II)–S-, –O are chemical bonds in Fe(II) sulfide and oxide.

*** The totals of all species of Fe and S are assumed to be one.

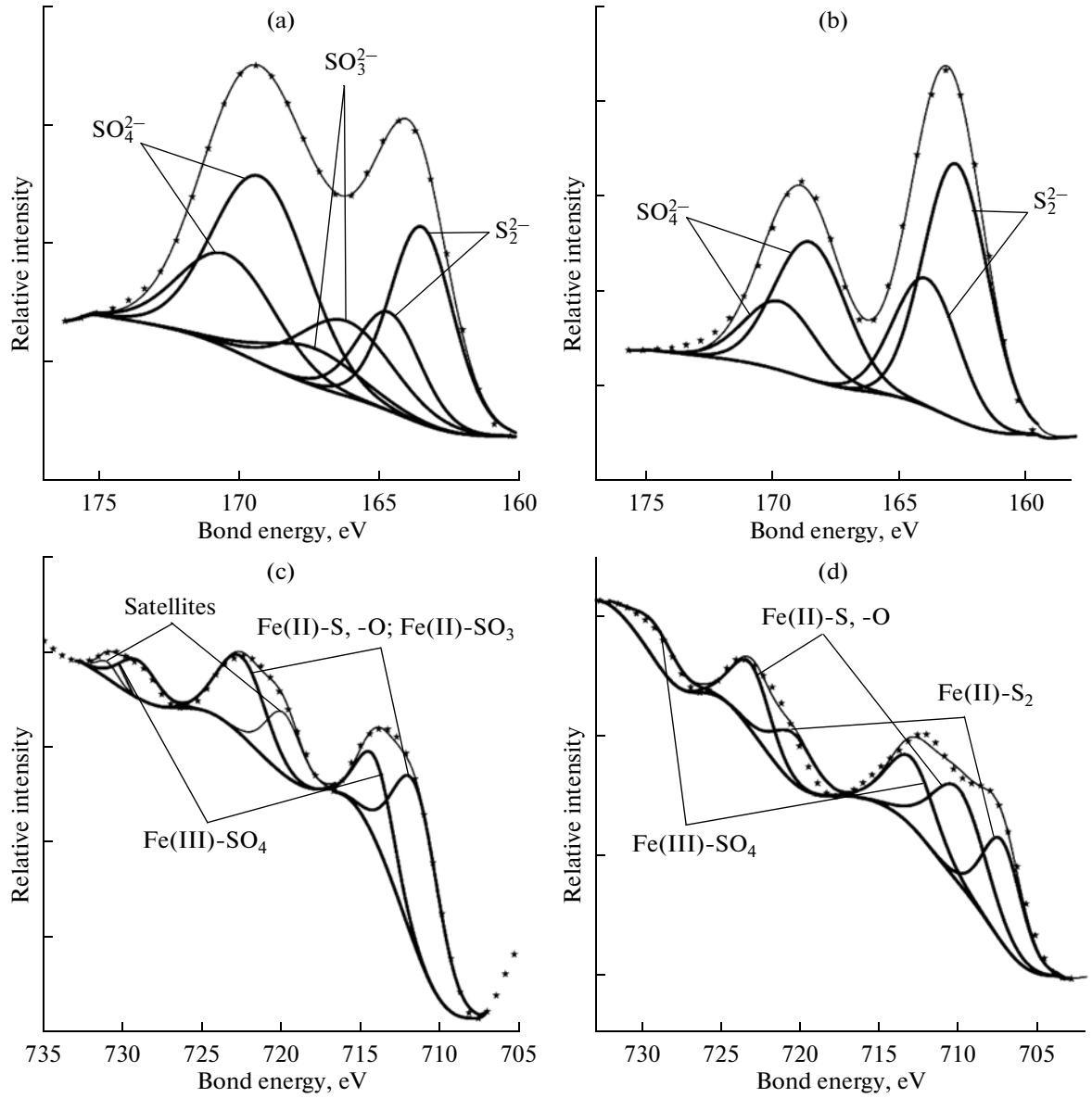

Fig. 6. XPS spectra of (a, b) S and (c, d) Fe for sample VPP-1/08-2 shkh. (a, c) Original sample, (c, d) after Ar^+ ion milling for 0.5 h. See Table 6 for the identification of the peaks. Line with small circles correspond to experiment data and their approximation. Heavy lines are deconvolution of the spectra. Satellites (not listed in Table 6) likely pertain to an admixture of Fe oxide in a high-spin state at the surface.

(Table 2), but their total mass is small. Larger crystals increase the Au concentration because of both structural and surface-related Au, but the latter ($\overline{C}_{sur}$) still remains dominant.

Close relations between active hydrothermal systems and epithermal deposits of precious metals are repeatedly emphasized in the literature (Williams-Jones and Heinrich, 2005; Pope et al., 2005). In view of this, it is interesting to compare the data on Au speciation presented in this publication with results obtained using the same techniques for epithermal Au–Ag deposits in northeastern Russia and mesothermal Au deposits in the Zun-Kholba Range in the Eastern Sayan Range (Tauson and Lipko, 2013). The proportions of structural and surface-related Au species in pyrite from hydrothermal clays in southern Kamchatka vary from 0.04 to 0.14. In the budget of species pertaining to evenly distributed ("invisible") gold, the structural mode makes up 3–12%, whereas 88–97% of the invisible Au is contained in surface-related modes. The concentrations of structural Au (0.07–0.25 ppm) are generally notably lower than in pyrite from orebodies (0.17–4.8 ppm) but higher than in pyrite from the wall-rock metasomatites (0.01–0.02 ppm). The concentrations of surface-related Au modes in pyrite from various mineral deposits broadly vary, from 1.5 to 60 ppm. In pyrite from

Table 7. Bulk S and Au concentrations in hydrothermal clays in the samples and Au concentrations in the pyrite

Sample	S, wt %	FeS_2, wt %	Au, ppm		
			analysis	calculation*	
				str.	sur.
VK-1/09-2	3.97	7.42	n.d.	0.01	0.19
VK-1/09-3	6.45	12.06	"	0.03	0.82
VPP-1/08-2 shkh	2.1	3.93	0.01	0.005	0.03
VPP-1/08-3 shkh	2.73	5.1	0.01	0.006	0.04
VPP-1/08-4 shkh	1.71	3.2	0.02	0.002	0.06
VPP-1/08-5 shkh	0.48	0.9	0.04	0.002	0.01

* Concentrations of the structural and surface-related modes of Au occurrence.

hydrothermal clays in Kamchatka, this range is narrower: 0.8–6.8 ppm. The source of ore components (Au, Fe, and S) for the wall-rock metasomatites was likely the host rocks, which were affected by Au-poor surface solutions heated by a deep-seated heat source during the premineral episode. If pyrite containing 0.01–0.02 ppm structural Au was formed as a result of this interaction, the somewhat higher Au concentrations in pyrite from the hydrothermal clays may be indicative of the involvement of juvenile (magmatic) fluid whose Au concentrations were higher than in the meteoric waters. However, these concentrations are in fact very low. Data on the Au concentrations in hydrothermal solutions at the Lower Koshelevskoe geothermal field ($1.8–4.5 \times 10^{-3}$ μg/l or approximately $1.8–4.5 \times 10^{-6}$ ppm) suggest very high Au enrichment coefficients of pyrite: some $n \times 10^4$ for the structural and $n \times 10^5$ for surface-related Au modes. Thus, compared to what is typical of higher parameters (450°C and 1 kbar; Tauson et al., 2011), Au not only becomes an element compatible with pyrite, but it becomes highly compatible with this mineral: the distribution coefficient of the structural mode D_{Au}^{str} increases from approximately $\sim 10^{-1}$ to roughly $\sim 10^4$, i.e., by five orders of magnitude, and D_{Au}^{bulk} further increases by one more order of magnitude because Au accumulation on the surface. Similar data on Au fractionation into a solid phase were obtained by studying hot springs in the Waiotapu area in North Island, New Zealand (Pope et al., 2005). In this instance, the enrichment factor ranges from $\sim 10^6$ to 10^8. The variations in the Au concentration were from $\sim 10^{-7}$ to 3.7×10^{-4} ppm in the liquid phase and from 9.2 to 543 ppm in the precipitate. These results were explained by Au adsorption and coprecipitation with As and Sb sulfides, although the amounts of these sulfides were too low to decrease the Au concentration in the solution to such low values. An important conclusion is that the effect of such processes at a certain depth cannot be ruled out (Pope et al., 2005). Hence, the sampled fluid has already partly discharged its load. Judging from the composition of fluid inclusions, Au concentrations in magmatic hydrothermal fluids can be of the order of a few ppm (Williams-Jones and Heinrich, 2005).

The reasons for which pyrite (this publication) and other minerals (Pope et al., 2005) with elevated Au concentrations (including those of structural Au modes) could crystallize from a depleted fluid are very important in the context of both the theory of epithermal ore-forming processes and exploration for Au deposits related to modern or ancient hydrothermal systems. We are prone to believe that the growth mechanisms of pyrite crystals undergo principal changes near the surface. The crystals grew there via incorporating colloid and subcolloid particles, and this resulted in a block microstructure of these crystals. If the sizes of the blocks are similar to those of the growth units (~50 to 100 nm), then calculations at 100°C indicate an increase in the Au concentration in a block crystal by two to three orders of magnitude depending on the size of the blocks and characteristics of dislocation boundaries of the blocks (Tauson et al., 1996). Correspondingly, the Au distribution coefficient between the pyrite and liquid phase should also increase by two to three orders of magnitude, if the liquid phase is visualized as a reservoir of infinite capacity with respect to the crystalline phases (which pertains to flow-through systems). It is important to emphasize the following two issues. First, Au is accommodated in the structure of a crystal, although this takes place in defective domains of the crystal impacted by the elastic fields of the dislocation boundaries. Second, this effect is enhanced with decreasing temperature (Urusov et al., 1997), and hence, a metal thus uptaken cannot be later discharged (in the form of, for example, Au°) when the system cools. This can take place only if the crystals are heated for a long enough

time, their defects are annealed, and the boundaries between their blocks are destructed. Another important characteristic of the mineral is Au accommodation in nonometer-sized surface phases. The latter can uptake the metal that occurs in excess when elemental growth units (colloid and subcolloid particles) are formed. Thereby other elements adsorbed by these particles (for example, Ti) can be brought to the surface. Physical and compositional characteristics of the surface phases are principally different from those determined previously in pyrite synthesized in hydrothermal experiments and found at ore deposits of various type (Tauson et al., 2008; Tauson and Lipko, 2013). They are richer in oxidized (sulfate and sulfite) than monosulfide sulfur, their structures are less ordered, less dense, they are porous, and their dominant morphology is globular (Table 4, Figs. 2–5). This highlights the typomorphism of the surface of low-temperature (~60–100°C) pyrite in hydrothermal clays. This conclusion is important for exploration mineralogy. As was demonstrated above, Au-bearing pyrite can account for much (if not all) Au contained in clayey and silicic sedimentary rocks at thermal fields (Table 7). Pyrite separated from such rocks can be easily mistaken for ore pyrite or this mineral in the wall-rock metasomatites. Analysis of modes of Au occurrence in this mineral can perhaps not reveal any appreciable differences from pyrite at gold deposits, and it is thus particularly important to study such characteristics of crystal surfaces as their morphology and composition, and parameters of the submicroscopic structure. If these aspects are not taken into consideration, some spurious anomalies can be found, which are not formed by high-temperature hydrothermal fluids that had an ore-forming potential, as is the case with the enrichment of ore metals in sublimates of high-temperature fumaroles (Kavalieris, 1994).

Returning to the problem of very high Au enrichment coefficients, it is pertinent to mention that, according to data in Table 6, the sizes of the blocks of pyrite crystals are greater than 100 nm and 170–230 nm. This means that dislocation-related Au uptake can hardly explain the five to six orders of magnitude greater values of D_{Au}^{bulk}. A consistent hypothesis able to reconcile these facts (high enrichment coefficient in the volume of the crystals and Au fractionation to their surface) is Au adsorption on the surface of FeS_2 colloid particles in the form of clusters consisting of a few atoms. They are concentrated in extension domains of the crystal lattice of pyrite, such as dislocation walls, which are formed if FeS_2 colloid particles are conjugated and (dominantly) at boundaries with coherent or semocoherent stressed surface phases (Akimov and Tauson, 1995). Such clusters in defective structural domains can be identified using techniques of transmission electron microscopy.

CONCLUSIONS

1. Pyrite is the main mineral concentrating Au in hydrothermal clays at the Upper Koshelevskoe and East Pauzhetka thermal fields in southern Kamchatka. The mineral contains Au evenly distributed over the volume of its crystals, in a structural mode (0.07–0.25 ppm), and Au in modes related to the surface of pyrite crystals (0.6–6.8 ppm).

2. The dependence of the concentration of evenly distributed Au on the specific surface area of an average crystal in a size fraction has high determination coefficients: $R^2 = 0.934–0.007$. A similarly clear dependence on the topological surface area of single crystals, and the absence of correlation with the "bulk" BET specific surface area, rules out purely sorption mechanisms of Au uptake by the surface of pyrite crystals, because in this situation, the concentrations of the minor element would have been proportional to the actual surface area (calculated with regard for the relief of the surface and its roughness) but not the topological one (determined with regard only for the geometry of the crystal polyhedrons).

3. In contrast to high-temperature hydrothermal systems, at lower temperature geothermal fields (whose temperatures is ~60–100°C), gold is an element highly compatible with pyrite. This results from a change in the growth mechanisms of pyrite crystals and the transition to crystal growth by means of incorporating colloid and subcolloid particles, as also follows from microscopic data and the change in the size of crystal blocks.

4. Low-temperature pyrite from hydrothermal clays shows certain typochemical features that are important for exploration for gold deposits related to modern or ancient geothermal systems. This pyrite differs from this mineral that crystallized at higher temperatures in bearing more widely spread sulfoxide sulfur compounds (as opposed to monosulfides species) and also in having a less ordered and dense structure, higher porosity, and a globular morphology of crystal surfaces. In the context of exploration mineralogy, it is important to take into account the morphology and composition of the surface of pyrite crystals when false anomalies can be found that are not related to high-temperature hydrothermal fluids having an ore-forming potential.

5. A high coefficient of Au enrichment in the volume of pyrite crystals and even higher coefficients of Au enrichment at their surface can likely be explained by Au adsorption on the surface of FeS_2 colloid particles in the form of clusters consisting of atomic groups. These groups are concentrated at extension domains of the pyrite crystal structure, such as dislocation walls, which are formed if colloid particles merged and also (and mostly) at boundaries with coherent or semicoherent stressed surface phases. We cannot rule out the effect of colloid particles of other composition (not FeS_2) that occur at the surface of pyrite crystals, although this problem deserves further exploration.

ACKNOWLEDGMENTS

The authors thank T.M. Pastushkova and T.S. Krasnoshchekova for help with analytical studies and Yu.V. Shchegol'kova for help with the spectroscopic research. This study was financially supported by the Russian Foundation for Basic Research (project nos. 12-05-00144, 12-05-98957-r_Siberia, 12-05-31004_mol, 12-05-31343_mol, and 13-05-002262) and the Siberian Branch of the Russian Academy of Sciences.

REFERENCES

V. V. Akimov and V. L. Tauson, "Compulsory equilibrium and pseudomorphism: a theory of pseudomorphic systems," Geokhimiya, No. 11, 1570–1585 (1995).

I. Kavalieris, "High Au, Ag, Mo, Pb, V and W content of fumarolic deposits at Merapi volcano, central Java, Indonesia," J. Geochem. Explor. **50** (1–3), 479–491 (1994).

J. G. Pope, K. L. Brown, and D. M. McConchie, "Gold concentrations in springs at Waiotapu, New Zealand: implications for precious metal deposition in geothermal systems," Econ. Geol. **100** (4), 677–687 (2005).

S. N. Rychagov, R. G. Davletbaev, O. V. Kovina, and G. P. Koroleva, "Characteristics of subsurface horizon of hydrothermal clays of the Nizhnii Koshelev and Pauzhetka geothermal deposits," Vestn. KRAUNTs, Ser. Nauki Zemle **12** (2), 116—134 (2008).

S. N. Rychagov, V. N. Sokolov, and M. S. Chernov, "Hydrothermal clays as a highly dynamical colloid–disperse mineralogical–geochemical system," Dokl. Earth Sci. **435** (2), 1684–1687 (2010).

S. N. Rychagov, V. N. Sokolov, and M. S. Chernov, "Hydrothermal clays of the geothermal fields of South Kamchatka: a new approach and study results," Geochem. Int. **50** (4), 344–357 (2012).

V. L. Tauson and E. E. Lustenberg, "Quantitative determination of modes of gold occurrence in minerals by the statistical analysis of analytical data samplings," Geochem. Int. **46** (4), 423-428 (2008).

V. L. Tauson and S. V. Lipko, "Pyrite as a concentrator of gold in laboratory and natural systems: a surface-related effect," in *Pyrite: Synthesis, Characterization and Uses*, Ed. by N. Whitley and P. T. Vinsen (Nova Sci. Pub., New York, 2013), pp. 1–40.

V. L. Tauson, D. N. Babkin, E. E. Lustenberg, S. V. Lipko, and I. Yu. Parkhomenko, "Surface typochemistry of hydrothermal pyrite: electron spectroscopic and scanning probe microscopic data. I. Synthetic pyrite," Geochem. Int. **46** (6), 565–577 (2008).

V. L. Tauson, D. N. Babkin, T. M. Pastushkova, T. S. Krashoshchekova, E. E. Lustenberg, and O. Yu. Belozerova, "Dualistic distribution coefficients of elements in the system mineral–hydrothermal solution. I. Gold accumulation in pyrite," Geochem. Int. **49** (6), 568–577 (2011).

V. L. Tauson, J. Goettlicher, A. N. Sapozhnikov, S. Mangold, and E. E. Lustenberg, "Sulphur speciation in lazurite-type minerals $(Na,Ca)_8[Al_6Si_6O_{24}](SO_4,S)_2$ and their annealing products: a comparative XPS and XAS study," Eur. J. Mineral. **24** (1), 133–152 (2012).

V. L. Tauson, A. G. Mironov, N. V. Smagunov, N. G. Bugaeva, and V. V. Akimov, "Gold in sulfides: the state of the mode of occurrence problem and prospects of experimental studies," Geol. Geofiz. **37** (3), 3–14 (1996).

V. L. Tausov, "Systematics of processes of trace element uptake by real mineral crystals," Geochem. Int. **43** (2), 184–190 (2005).

V. S. Urusov, V. L. Tauson, and V. V. Akimov, *Solid State Geochemistry* (GEOS, Moscow, 1997) [in Russian].

A. E Williams-Jones and C. A. Heinrich, "Vapor transport of metals and the formation of magmatic-hydrothermal ore deposits," Econ. Geol. **100** (7), 1287–1312 (2005).

Translated by E. Kurdyukov

SPELL: OK